

1 Title

2 Bias correction of gauge-based gridded product to improve extreme precipitation analysis in the
3 Yarlung Tsangpo-Brahmaputra River Basin

4

5 Author names and affiliations

6 Xian Luo^{1,2}, Xuemei Fan¹, Yungang Li^{1,2}, and Xuan Ji^{1,2}

7 ¹Institute of International Rivers and Eco-security, Yunnan University, Kunming, China

8 ²Yunnan Key Laboratory of International Rivers and Transboundary Eco-security, Kunming, China

9

10 Address

11 Institute of International Rivers and Eco-security, Yunnan University,

12 South Section, East Outer Ring Road, Chenggong District, Kunming, China

13

14 Email

15 Xian Luo: luoxian@ynu.edu.cn

16 Xuemei Fan: fanxuemei7@163.com

17 Yungang Li: ygli@ynu.edu.cn

18 Xuan Ji: jixuan@ynu.edu.cn

19

20 Contact Author: Xian Luo (luoxian@ynu.edu.cn)

21 Second Contact Author: Yungang Li (ygli@ynu.edu.cn)

22

23 **Abstract.** Critical gaps in the amount, quality, consistency, availability, and spatial distribution of
24 rainfall data limit extreme precipitation analysis, and the application of gridded precipitation data
25 are challenging because of their considerable biases. This study corrected Asian Precipitation Highly
26 Resolved Observational Data Integration Towards Evaluation of Water Resources (APHRODITE)
27 estimates in the Yarlung Tsangpo-Brahmaputra River Basin (YBRB) using two linear and two
28 nonlinear methods, and their influence on extreme precipitation indices were assessed by cross-
29 validation. Bias correction greatly improved the performance of extreme precipitation analysis. The
30 ability of four methods to correct wet-day frequency and coefficient of variation were substantially
31 different, leading to considerable differences in extreme precipitation indices. Local intensity
32 scaling (LOCI) and quantile–quantile mapping (QM) performed better than linear scaling (LS) and
33 power transformation (PT). This study would provide reference for using gridded precipitation data
34 in extreme precipitation analysis and selecting bias-corrected method for rainfall products in data-
35 sparse regions.

36

37 **1 Introduction**

38 Extreme precipitation often leads to floods, debris flows, and other secondary disasters (Wang
39 et al., 2017), and changes in the frequency and intensity of extreme precipitation profoundly
40 influence both natural environment and human society profoundly (Easterling et al., 2000; Yucel
41 and Onen, 2014). Rainfall observations provide a primary foundation for comprehending their long-
42 term variability and change in extreme precipitation (Alexander, 2016). Accurate rainfall data are
43 necessary for flood protection and water resource management. However, due to scarce spatial
44 coverage of rainfall stations, short-length rainfall records, and high proportions of missing data,

45 observations currently available in some remote basins are clearly inadequate to capture their
46 precipitation characteristics. In addition, observed rainfall data are usually difficult to collect in
47 international river basins because many countries may not share or freely distribute data (Lakshmi
48 et al., 2018).

49 The Yarlung Tsangpo-Brahmaputra River is the fourth largest river in the world in terms of
50 flow (Kamal-Heikman et al., 2007), which is influenced profoundly by complex atmospheric
51 dynamics and regional climate processes (Immerzeel et al., 2010; Pervez and Henebry, 2015).
52 Because its agriculture and economy rely heavily on monsoon precipitation, the basin is particularly
53 vulnerable to changing climate (Singh et al., 2016; Liu et al., 2018; Janes et al., 2019; Xu et al.,
54 2019; Zhang et al., 2019). During the four summer monsoon months of June, July, August, and
55 September (JJAS), extreme precipitation with large uncertainties lead to numerous floods (Kamal-
56 Heikman et al., 2007; Dimri et al., 2016; Malik et al., 2016). However, the understanding on extreme
57 precipitation in the Yarlung Tsangpo-Brahmaputra River Basin (YBRB) have a number of gaps
58 because of its complex topographic interactions with atmospheric flows, lack of observations, and
59 data sharing issues, which hinder effective flood management (Ray et al., 2015; Prakash et al., 2019).

60 Currently, different gridded rainfall products provide effective information over regional to
61 global scales, which could be broadly classified into four categories: (1) gauge-based data sets that
62 build on observations from rainfall stations; (2) products from numerical weather predictions or
63 atmospheric models; (3) satellite-only products; and (4) combined satellite-gauge products. The
64 performance of these products vary from region to region (Duan et al., 2016). Given the
65 heterogeneity of orography and climate in the YBRB, observing and modeling its precipitation are
66 very challenging (Khandu et al., 2017). In addition, satellite products are less reliable because high

67 convective rainfall generally takes place in the southern foothills of the Himalayas (Prakash et al.,
68 2015). Compared with some other gauge-based products, Asian Precipitation Highly Resolved
69 Observational Data Integration Towards Evaluation of Water Resources (APHRODITE) dataset
70 collected more rainfall observations across South Asia (Rana et al., 2015), which have been proved
71 could better estimate spatial precipitation (Andermann et al., 2011). Nonetheless, the lack and
72 uneven distribution of rainfall stations at high altitudes in the Tibetan Plateau and Himalayas may
73 introduce uncertainty and affect the accuracy of APHRODITE estimates (Rana et al., 2015;
74 Chaudhary et al., 2017).

75 Numerous rainfall observations can be obtained from public databases, although their short
76 record and static character limit their direct application in precipitation analysis (Donat et al., 2013).
77 However, these data could be useful for bias correction of gauge-based gridded products by
78 providing additional observations from the denser network of rainfall stations. On the other hand,
79 ranging from simple linear scaling to more sophisticated nonlinear approaches, several methods
80 have been developed to adjust global climate model (GCM) data (Teutschbein and Seibert, 2012).
81 Similarly, these bias correction methods could be applied to correct gridded rainfall products in
82 sparsely-gauged mountainous basins (He et al., 2017). It is important to study whether extreme
83 precipitation analysis could be improved by bias correction of gridded precipitation data and how
84 different methods would influence extreme precipitation indices.

85 This study evaluated different bias correction approaches for APHRODITE estimates in the
86 YBRB and assessed their effects on extreme precipitation analysis. We first corrected APHRODITE
87 estimates by both linear and nonlinear methods. Next, we calculated extreme precipitation indices
88 using original and different corrected APHRODITE estimates, and the effects of bias correction on

89 extreme precipitation analysis were further investigated by cross-validation. The results would
90 support reference for the application of gridded precipitation data and bias-corrected methods in
91 extreme precipitation analysis.

92

93 **2 Material and methods**

94 **2.1 Study area**

95 The YBRB can be divided into three physiographic zones: (1) the Tibetan plateau (TP),
96 covering 44.4% of the basin, with elevations above 3500 m; (2) the Himalayan belt (HB), accounting
97 for 28.6% of the basin, with elevations ranging from 100 m to 3500 m; and (3) the floodplains (FP),
98 covering 27.0% of the basin, with elevations up to 100 m (Immerzeel, 2008).

99 The moisture in the YBRB is mainly from the Indian Ocean. The YBRB exhibits a broad range
100 of precipitation from the semi-arid upstream areas to the HB characterized by abundant orographic
101 rainfall as well as the vast humid FP. In the upstream areas, precipitation is concentrated during
102 JJAS, and rainfall intensity is mostly low due to long-distance moisture transport (Guan et al., 1984).
103 The irregular topographic variations in the Himalayas profoundly affect the spatial distribution of
104 precipitation by altering monsoonal flow, producing intense orographic rainfall along the Himalayan
105 foothills (Khandu et al., 2017). The downstream areas also receive high rainfall from monsoon flow
106 during JJAS, accounting for 60%–70% of the annual rainfall (Gain et al., 2011).

107

108 **2.2 Data sources**

109 **2.2.1 Observational data**

110 In the upper YBRB, rainfall data across China recorded at 31 meteorological stations were

111 collected from the National Meteorological Information Center (NMIC, sourced from the China
112 Meteorological Data Sharing Service System). In addition, data observed at 91 rainfall stations in
113 the downstream area were obtained from the Global Historical Climatology Network
114 (GHCN)–Daily dataset for bias correction. GHCN-Daily dataset comprises observations from four
115 sources, which have been undergone extensive quality reviews, including the U.S. Collection, the
116 International Collection, the Government Exchange Data, and the Global Summary of the Day. The
117 locations of rainfall stations are shown in Fig. 1.

118

119 **2.2.2 APHRODITE estimates**

120 Numerous rainfall observations were incorporated into APHRODITE estimates, including (1)
121 Global Telecommunication System (GTS)-based data, (2) data obtained from other projects or
122 organizations, and (3) their own collection. The rainfall observations that had undergone quality
123 control were gathered, and the ratios of rainfall observations to the world climatology were
124 calculated and then interpolated for each month. The interpolated ratios were multiplied by the world
125 climatology, and the first six components of the fast Fourier transform of the resulting values were
126 used to obtain daily precipitation (Yatagai et al., 2012).

127 Daily rainfall data of APHRO_MA_025deg_V1101 ([http://aphrodite.st.hirosaki-](http://aphrodite.st.hirosaki-u.ac.jp/index.html)
128 [u.ac.jp/index.html](http://aphrodite.st.hirosaki-u.ac.jp/index.html)) at 0.25° resolution in the Asian monsoon area end in 2007, while recently
129 published APHRO_MA_025deg_V1101EX_R1 (<http://aphrodite.st.hirosaki-u.ac.jp/index.html>),
130 using the same algorithm and spatial resolution, extend the time series over the period 2007–2015.
131 Therefore, extreme precipitation could be analyzed during 1951–2015 by applying both datasets.
132 To investigate the influence of topography on bias-corrected APHRODITE estimates, the grids were

133 classified into three topographic zones (the TP, HB, and FP; Fig. 2).

134

135 **2.3 Methods**

136 **2.3.1 Bias correction methods**

137 Two linear methods (linear scaling (LS) and local intensity scaling (LOCI)) and two non-linear
138 methods (power transformation (PT) and quantile–quantile mapping (QM)) were used for bias
139 correction in this study.

140 (1) LS

141 LS corrects monthly estimates in accordance with observations (Lenderink et al., 2007). It
142 corrects APHRODITE estimates using the ratio between mean monthly observation and
143 corresponding estimation:

$$144 \quad P_{APH}^*(d) = P_{APH}(d) \cdot \left[\frac{\mu_m(P_{obs}(d))}{\mu_m(P_{APH}(d))} \right] \quad (1)$$

145 where $P_{APH}^*(d)$ and $P_{APH}(d)$ are the daily precipitation of corrected and original APHRODITE
146 estimate, respectively, and $P_{obs}(d)$ is the daily precipitation observed at the rainfall station in
147 corresponding grid of the APHRODITE estimate. $\mu_m(P_{obs}(d))$ and $\mu_m(P_{APH}(d))$ are the mean
148 monthly precipitation of observations and corresponding APHRODITE estimates in the m th month,
149 respectively.

150 (2) LOCI

151 LOCI makes a flexible adjustment to the wet-day frequency and intensity (Schmidli et al., 2006;
152 Teutschbein and Seibert, 2012). Firstly, an adjusted precipitation threshold ($P_{th,APH}$) is determined so
153 that the number of days exceeding this threshold for APHRODITE estimates matches that of
154 observed days with precipitation larger than 0 mm. Secondly, a linear scaling factor (s) for wet days

155 is computed:

$$156 \quad s = \frac{\mu_m(P_{obs}(d)|P_{obs}(d) > 0 \text{ mm})}{\mu_m(P_{APH}(d)|P_{APH}(d) > P_{th,APH}) - P_{th,APH}} \quad (2)$$

157 where $\mu_m(P_{obs}(d)|P_{obs}(d) > 0 \text{ mm})$ is the mean monthly precipitation of observations with daily

158 precipitation larger than 0 mm, and $\mu_m(P_{APH}(d)|P_{APH}(d) > P_{th,APH})$ is the mean monthly precipitation

159 of APHRODITE estimates with daily precipitation larger than $P_{th,APH}$. Finally, the precipitation data

160 are corrected, using:

$$161 \quad P_{APH}^*(d) = \max(s \cdot (P_{APH}(d) - P_{th,APH}), 0) \quad (3)$$

162 (3) PT

163 PT corrects both the mean and the coefficient of variation of precipitation (Leander and

164 Buishand, 2007), changing precipitation by:

$$165 \quad P_{APH}^*(d) = a \cdot (P_{APH}(d))^b \quad (4)$$

166 where a and b are the parameters of the power transformation, which are obtained using a

167 distribution-free approach and estimated for each month within a 90-day window. Using a root-

168 finding algorithm, the value of b is firstly determined to ensure that the coefficient of variation of

169 the corrected estimates matches that of the observations. The parameter a is then calculated using

170 the mean observation and the corresponding mean of the transformed values.

171 (4) QM

172 By shifting occurrence distributions, QM corrects the distribution function of precipitation

173 estimates to match that of observations, which is commonly used in correcting systematic

174 distributional biases (Cannon et al., 2015). A Gamma distribution is usually assumed for

175 precipitation events (Teutschbein and Seibert, 2012):

176 $f_{\gamma}(x|\alpha, \beta) = x^{\alpha-1} \cdot \frac{1}{\beta^{\alpha} \cdot \Gamma(\alpha)} \cdot e^{-\frac{x}{\beta}}; x \geq 0; \alpha, \beta > 0$ (5)

177 where α and β are the shape parameter and scale parameter, respectively.

178 The cumulative density function (CDF) of the APHRODITE estimates is adjusted to agree with
 179 that of the observation, and the daily precipitation for APHRODITE estimates is corrected
 180 depending on its quantile. It should be noted that for APHRODITE estimates, many days had low
 181 precipitation estimates instead of substantial dry conditions, which may distort the distribution of
 182 daily precipitation. Therefore, an adjusted precipitation threshold is also used to ensure the wet-day
 183 frequency of corrected APHRODITE estimates match the observed frequency:

184
$$P_{APH}^*(d) = \begin{cases} 0, & \text{if } P_{APH}(d) < P_{th,APH} \\ F_{\gamma}^{-1}(F_{\gamma}(P_{APH}(d)|\alpha_{APH,m}, \beta_{APH,m})|\alpha_{obs,m}, \beta_{obs,m}), & \text{otherwise} \end{cases}$$

185 (6)

186 F_{γ} and F_{γ}^{-1} are the Gamma CDF and its inverse, respectively. $\alpha_{APH,m}$ and $\beta_{APH,m}$ are the shape
 187 parameter and scale parameter of original APHRODITE estimates in the m th month, respectively,
 188 and $\alpha_{obs,m}$ and $\beta_{obs,m}$ are those of observations in the m th month, respectively.

189 This study corrected the grids of the APHRODITE estimates that contained time series of
 190 observations, and the parameters of bias correction were determined using corresponding available
 191 rainfall observations. After that, the APHRODITE estimates during 1951–2015 in these grids were
 192 corrected by 4 bias correction methods, respectively. Hereafter, APHRODITE estimates corrected
 193 by LS, LOCI, PT, and QM are referred as LS-APHRODITE, LOCI-APHRODITE, PT-
 194 APHRODITE, and QM-APHRODITE estimates, respectively.

195

196 2.3.2 Indices of extreme precipitation

197 To characterize extreme precipitation during JJAS, six indices recommended by the Expert

198 Team on Climate Change Detection and Indices (ETCCDI), including consecutive wet days (CWD),
199 number of heavy precipitation days (R10mm), number of very heavy precipitation days (R20mm),
200 maximum 1-day precipitation amount (Rx1d), maximum 5-day precipitation amount (Rx5d), and
201 simple daily intensity index (SDII), were applied in this study. Detailed descriptions of these indices
202 are shown in Table 1. The indices fall roughly into three categories: (1) duration indices, which
203 represent the length of the wet spell; (2) threshold indices, which count the days on which a fixed
204 precipitation threshold is exceeded; (3) absolute indices, which describe the maximum 1-day or 5-
205 day precipitation amount (Sillmann et al., 2013).

206 Extreme precipitation indices for corrected APHRODITE estimates in the grids distributed
207 with rainfall stations were calculated. To obtain extreme precipitation indices in other grids, inverse
208 distance weighted (IDW) interpolation for extreme precipitation indices were performed. This
209 allowed us to calculate mean values for each of the three topographic zones.

210

211 **2.3.3 Validation on bias correction**

212 Cross-validation was used to evaluate the performance of 4 bias correction methods. At each
213 rainfall station, the observations were divided into two groups. Two third of the rainfall records were
214 applied to calculate the parameters of bias correction, and then APHRODITE estimates were
215 corrected. Making use of the remaining rainfall observations, the mean error (*ME*) of the extreme
216 precipitation indices for corrected APHRODITE estimates were calculated to evaluate the
217 performance of different bias correction methods.

218

219 **3 Results**

220 **3.1 Extreme precipitation indices calculated from original and corrected APHRODITE**
221 **estimates**

222 **3.1.1 Extreme precipitation indices in the three physiographic zones**

223 Extreme precipitation indices calculated from original and four corrected APHRODITE
224 estimates in the three different physiographic zones are shown in Fig. 3. The CWD estimated using
225 original APHRODITE and LS-APHRODITE estimates were similar. Meanwhile, those derived
226 from LOCI-, PT-, and QM-APHRODITE estimates were much less.

227 Mean R10mm during JJAS obtained by original APHRODITE estimates in the TP, HB, and FP
228 were 6.7, 31.0, and 47.7 days, respectively. These were similar to those estimated by corrected
229 APHRODITE estimates. However, the differences in R20mm were much pronounced. Mean
230 R20mm in HB and FP for bias-corrected APHRODITE datasets were close to 19.0 and 26.5 days,
231 respectively, which were approximately 4–5 days higher than those derived from original
232 APHRODITE estimates.

233 Compared with original APHRODITE estimates, the Rx1d and Rx5d increased greatly after
234 bias correction. In the HB, the mean Rx1d obtained from original APHRODITE estimates was 49.5
235 mm, while those for LS-, LOCI-, PT-, and QM-APHRODITE estimates were 72.4, 90.1, 109.0, and
236 103.8 mm, respectively. In addition, the ranges of Rx1d and Rx5d also increased considerably.

237 The differences in SDII between original and corrected APHRODITE estimates were also
238 marked. For example, mean SDII in the FP calculated from original APHRODITE estimates was
239 13.4 mm. After correction, mean SDII for LOCI- and QM-APHRODITE estimates increased to 23.4
240 and 25.1 mm, respectively. These values were much greater than those derived from LS- and PT-
241 APHRODITE datasets (15.7 and 17.7 mm).

242

243 **3.1.2 Relative changes in extreme precipitation indices**

244 The relative changes in extreme precipitation indices during JJAS based on original and
245 corrected APHRODITE estimates are shown in Fig. 4. The CWD for LOCI-, PT-, and QM-
246 APHRODITE estimates were all lower than original APHRODITE estimates, yielding relative
247 change rates from -66% to -27% . Bias correction decreased the number of rainy days except LS.
248 The variations in R10mm and R20mm illustrated that corrected APHRODITE estimates identified
249 much more extreme precipitation events in the TP. The changes in indices varied considerably for
250 different correction methods, with the change rates of R20mm in the TP for LS-, LOCI-, PT-, and
251 QM-APHRODITE estimates being 30.4% , 169.2% , 297.1% , and 317.4% , respectively. For Rx1d,
252 Rx5d, and SDII, the increases in the HB were much pronounced than those in the FP and TP. Except
253 for LS-APHRODITE estimates, the increases in Rx1d and Rx5d in the HB were all above 70% for
254 corrected APHRODITE estimates.

255

256 **3.2 Influence of bias correction on extreme precipitation indices**

257 **3.2.1 Evaluation of extreme precipitation indices**

258 The *ME* of extreme precipitation indices during JJAS for validation are shown in Fig. 5. For
259 original APHRODITE estimates, the *ME* of CWD in the TP, HB, and FP were 8.3, 16.4, and 21.8
260 days, respectively. There were a lot of days with low precipitation estimations instead of substantial
261 dry conditions, leading to the overestimation on CWD. Likewise, this propagated to LS-
262 APHRODITE estimates with similar *ME* of CWD, because there was no change made to the wet-
263 day frequency. The *ME* of CWD in the TP, HB, and FP for LOCI-APHRODITE estimates were 3.1,

264 1.2, and 1.4 days, respectively, and those for QM-APHRODITE estimates were 2.5, 0.8, and 0.9
265 days, respectively. For both LOCI- and QM-APHRODITE estimates, the days with low
266 precipitation estimations instead of substantial dry conditions were redefined as dry days using
267 precipitation threshold, resulting in much less *ME* and more reliable CWD. Finally, although PT did
268 not directly correct wet-day frequency, the CWD for PT-APHRODITE estimates were lower than
269 those for original APHRODITE estimates because tiny precipitation were corrected.

270 Original APHRODITE tended to underestimate heavy and very heavy precipitation days. Bias
271 correction reduced error on R10mm and R20mm except LS, and the absolute value of mean *ME* for
272 LOCI-, PT-, and QM-APHRODITE estimates were mostly less than 1.0 days. LOCI, PT, and QM
273 are able to effectively correct heavy and very heavy precipitation days.

274 For original APHRODITE estimates, the *ME* of Rx1d were -11.3, -89.1 and -50.5 mm in the
275 TP, HB, and FP, respectively, and those of Rx5d reached -18.0, -167.4 and -76.8 mm, respectively.
276 Original APHRODITE estimates greatly underestimated Rx1d and Rx5d. For corrected
277 APHRODITE estimates, QM performed best on Rx1d, and the *ME* for QM-APHRODITE estimates
278 were -0.1, -1.9 and -5.4 mm, respectively. LS and LOCI used consistent ratio in linear
279 transformation, resulting in underestimation on Rx1d. In addition, LOCI outperformed other
280 methods on Rx5d, and the overestimation in the HB and FP for PT- and QM-APHRODITE estimates
281 were greater.

282 The *ME* of SDII for original APHRODITE estimates in the TP, HB, and FP were -2.4, -13.9
283 and -11.0 mm, respectively. Firstly, heavy and very heavy precipitation in the HB and TP were not
284 fully captured by original APHRODITE estimates. Secondly, original APHRODITE estimates
285 overestimated wet days, which distorted the estimation of precipitation intensity. Smaller error were

286 found in LOCI- and QM-APHRODITE estimates because they corrected rainfall amount as well as
287 the number of rainy days.

288

289 **3.2.2 Spatial distribution of extreme precipitation**

290 Rainstorms over the lower YBRB usually have the duration of 2–3 days (Dhar and Nandargi,
291 2000), and large multi-day precipitation events are crucial to the floods in the basin. Hence, the
292 spatial distribution of Rx5d during JJAS based on original APHRODITE estimates were compared
293 with corrected APHRODITE estimates in Fig. 6. For original APHRODITE estimates, the area with
294 Rx5d higher than 300 mm only accounted for 2.0% of the basin, while the proportions for LS-,
295 LOCI-, PT-, and QM-APHRODITE estimates were 10.9%, 18.7%, 21.7%, and 21.3%, respectively.
296 The most profound difference between original and corrected APHRODITE estimates occurred over
297 the windward slopes of the Himalayas before the river flows into the Brahmaputra valley. The Rx5d
298 calculated from original APHRODITE estimates were lower than 300 mm, while much higher Rx5d
299 were obtained after bias correction, yielding maxima of 946.6, 1030.3, 1105.1, and 1396.6 mm for
300 LS-, LOCI-, PT-, and QM-APHRODITE estimates, respectively. The eastern Himalayas, acting as
301 orographic barriers, push the southwest moist air upwards, leading to heavier extreme precipitation
302 over the windward slopes (Singh et al., 2004; Bookhagen and Burbank, 2010; Dimri et al., 2016).
303 However, original APHRODITE estimates tended to substantially underestimate these extreme
304 precipitation. Besides aforementioned region, higher Rx5d along the Himalayan front were also
305 found after bias correction. In this case, extreme precipitation calculated from nonlinear approaches
306 were heavier than those derived from linear methods. In general, bias correction are able to consider
307 topographic effects on the spatial distribution of extreme precipitation more comprehensively.

308

309 **4 Discussion**

310 Using two linear and two nonlinear bias methods, we corrected APHRODITE estimates during
311 JJAS in the YBRB to investigate the effects of different approaches on extreme precipitation
312 analysis. Extreme precipitation indices were strongly dependent on the bias correction approach
313 applied.

314 A primary problem when using gauge-based gridded data sets for extreme precipitation
315 analysis is the fundamental mismatch between point-based observations and gridded estimates
316 (Alexander, 2016). In addition, the spatial coverage of rainfall stations is another major source of
317 uncertainty, particularly where spatial distributions of precipitation are complex (Donat et al., 2013).
318 There are currently several approaches for bias correction, ranging from simple linear scaling to
319 more sophisticated nonlinear methods (Teutschbein and Seibert, 2012). Although mean precipitation
320 corrected by all bias-corrected approaches were similar, their standard deviations and consequent
321 extreme precipitation indices varied considerably. In the case of linear correction, both mean and
322 standard deviation are multiplied by same factor (Leander and Buishand, 2007), resulting in dubious
323 variations of precipitation. Nonlinear correction adjust mean and also coefficient of variation
324 (Teutschbein and Seibert, 2012), yielding more reliable results. In addition, the typical biases of
325 rainfall products are related to their identification of too many wet days with low-intensity
326 precipitation. Among the four bias-corrected approaches applied herein, LS and PT make no change
327 on the number of rainy days, while LOCI and QM use threshold exceedance to match the wet-day
328 frequency to the observations.

329 In international river basins, rainfall data are usually not publicly available, and extreme

330 precipitation analysis may suffer from data restrictions (Nishat and Rahman, 2009; Luo et al., 2019).
331 Several great international rivers in south Asia, including the Indus, Ganges, and Yarlung
332 Tsangpo–Brahmaputra, originate from or flow through the Himalayas. Topographic variations of
333 the Himalayas profoundly influence the spatial distribution of precipitation by altering monsoonal
334 flow, resulting in considerable orographic rainfall on the windward slopes (Khandu et al., 2017).
335 Rainfall estimates of different products varied markedly along the Himalayan front and obtained
336 similar results toward the adjacent low-relief domains (Andermann et al., 2011). The GHCN-Daily
337 data can be applied to correct gauge-based gridded data sets in this region, ensuring these products
338 capture the spatial distribution and variation of extreme precipitation. However, numerous GHCN-
339 Daily records in Asia do not contain data from recent years, and the short or incomplete rainfall
340 records limit their direct applications (Donat et al., 2013). Hence, it would be preferable to apply
341 nonpublic datasets in data-sparse regions.

342

343 **5 Conclusions**

344 Despite increasing use of gridded rainfall products in sparsely gauged river basins, their
345 application in extreme precipitation analysis is challenging due to considerable biases. This study
346 made use of four methods to correct APHRODITE estimates in the YBRB. Their influences on
347 extreme precipitation indices were compared and assessed. The following conclusions were drawn.

348 (1) Original APHRODITE estimates tended to underestimate heavy and very heavy
349 precipitation in the YBRB, and there were a lot of days with low precipitation estimations instead
350 of substantial dry conditions. Bias correction greatly improved the performance of extreme
351 precipitation analysis. The extreme precipitation indices calculated from different corrected

352 APHRODITE estimates varied substantially, and LOCI- and QM-APHRODITE estimates were able
353 to obtain more reliable extreme precipitation indices.

354 (2) Insufficient gauge observations in the Himalayas caused high uncertainty in the heavy
355 precipitation estimates for original APHRODITE estimates. After bias correction using observations
356 from a denser network of gauges, the heterogeneous orographic effects on extreme precipitation
357 were captured more accurately.

358

359 *Data availability.* The co-authors used publicly available data from the Asian Precipitation Highly
360 Resolved Observational Data Integration Towards Evaluation of Water Resources and the National
361 Centers for Environmental Information. In addition, rainfall observations in China were obtained
362 from the National Meteorological Information Center.

363

364 *Author contributions.* XL and YL conceived the study, XL and XF carried out bias correction and
365 extreme precipitation analysis, XL drafted the paper, and all co-authors jointly worked on enriching
366 and developing the draft.

367

368 *Competing interests.* The authors declare that they have no conflict of interest.

369

370 *Acknowledgements.* This study was supported by the National Natural Science Foundation of China
371 (41661144044, 41601026), the National Key R&D Program of China (2016YFA0601601), and the
372 Science and Technology Planning Project of Yunnan Province, China (2017FB073).

373

374 **References**

375 Alexander, L. V.: Global observed long-term changes in temperature and precipitation extremes: A
376 review of progress and limitations in IPCC assessments and beyond, *Weather & Climate Extremes*,
377 11, 4–16, <https://doi.org/10.1016/j.wace.2015.10.007>, 2016.

378 Andermann, C., Bonnet, S., and Gloaguen, R.: Evaluation of precipitation data sets along the
379 Himalayan front, *Geochemistry, Geophysics, Geosystems*, 12, Q07023,
380 <https://doi.org/10.1029/2011gc003513>, 2011.

381 Bookhagen, B., Burbank, and D. W.: Toward a complete Himalayan hydrological budget:
382 Spatiotemporal distribution of snowmelt and rainfall and their impact on river discharge, *Journal of*
383 *Geophysical Research*, 115, F03019, <https://doi.org/doi:10.1029/2009JF001426>, 2010.

384 Cannon A. J., Sobie S. R., Murdock T. Q.: Bias correction of GCM precipitation by quantile
385 mapping: How well do methods preserve changes in quantiles and extremes? *Journal of Climate*,
386 28, 6938–6959, <https://doi.org/10.1175/JCLI-D-14-00754.1>, 2015.

387 Chaudhary S., Dhanya C. T., and Vinnarasi R.: Dry and wet spell variability during monsoon in
388 gauge-based gridded daily precipitation datasets over India, *Journal of Hydrology*, 546, 204–218,
389 <https://doi.org/10.1016/j.jhydrol.2017.01.023>, 2017.

390 Dhar, O. N. and Nandargi, S.: A study of floods in the Brahmaputra Basin in India, *International*
391 *Journal of Climatology*, 20, 771–781, 2000.

392 Dimri, A. P., Thayyen, R. J., Kibler, K., Stanton, A., Jain, S. K., Tullos, D., and Singh, V. P.: A review
393 of atmospheric and land surface processes with emphasis on flood generation in the Southern
394 Himalayan rivers, *Science of the Total Environment*, 556, 98 – 115,
395 <http://dx.doi.org/10.1016/j.scitotenv.2016.02.206>, 2016.

396 Donat, M.G., Alexander, L.V., Yang, H., Durre, I., Vose, R., and Caesar, J.: Global land-based
397 datasets for monitoring climatic extremes, *Bulletin of the American Meteorological Society*, 94,
398 997–1006, <http://dx.doi.org/10.1175/BAMS-D-12-00109.1>, 2013.

399 Easterling, D. R.: Climate extremes: observations, modeling, and impacts, *Science*, 289, 2068–2074,
400 <https://doi.org/doi:10.1126/science.289.5487.2068>, 2000.

401 Gain, A. K., Immerzeel, W. W., Sperna Weiland, F. C., and Bierkens, M. F. P.: Impact of climate
402 change on the stream flow of the lower Brahmaputra: trends in high and low flows based on
403 discharge-weighted ensemble modelling, *Hydrology and Earth System Sciences*, 15, 1537–1545,
404 <https://doi.org/10.5194/hess-15-1537-2011>, 2011.

405 Guan, Z. H., Chen, C. Y., Ou, Y. X., Fan, Y. Q., Zhang, Y. S., Chen, Z. M., Bao, S. H., Zu, Y. T., He,
406 X. W., and Zhang, M. T. (Eds.): *Rivers and Lakes in Tibet*, Science Press, Beijing, China, pp. 35–
407 39, 1984.

408 He, Z., Hu, H., Tian F., Ni G., and Hu Q.: Correcting the TRMM rainfall product for hydrological
409 modelling in sparsely-gauged mountainous basins, *Hydrological Sciences Journal*, 62, 306–318,
410 <https://doi.org/10.1080/02626667.2016.1222532>, 2017.

411 Immerzeel, W.: Historical trends and future predictions of climate variability in the Brahmaputra
412 basin, *International Journal of Climatology*, 28, 243–254, <https://doi.org/10.1002/joc.1528>, 2008.

413 Immerzeel, W. W., van Beek, L. P. H., and Bierkens, M. F. P.: Climate change will affect the Asian
414 water towers, *Science*, 328, 1382–1385, <https://doi.org/10.1126/science.1183188>, 2010.

415 Janes, T., Mcgrath, F., Macadam, I., and Jones, R.: High-resolution climate projections for south
416 Asia to inform climate impacts and adaptation studies in the Ganges-Brahmaputra-Meghna and
417 Mahanadi deltas, *Science of The Total Environment*, 650, 1499 – 1520,

418 <https://doi.org/10.1016/j.scitotenv.2018.08.376>, 2019.

419 Kamal-Heikman, S., Derry, L. A., Stedinger, J. R., and Duncan, C. C.: A simple predictive tool for
420 lower Brahmaputra River Basin monsoon flooding, *Earth Interactions*, 11, 1 – 11,
421 <https://doi.org/10.1175/EI226.1>, 2007.

422 Khandu, Awange, J. L., Kuhn, M., Anyah, R., and Forootan, E.: Changes and variability of
423 precipitation and temperature in the Ganges-Brahmaputra-Meghna River Basin based on global
424 high-resolution reanalyses, *International Journal of Climatology*, 37, 2141–2159,
425 <https://doi.org/10.1002/joc.4842>, 2017.

426 Lakshmi, V., Fayne, J., and Bolten, J.: A comparative study of available water in the major river
427 basins of the world, *Journal of Hydrology*, 567, 510 – 532,
428 <https://doi.org/10.1016/j.jhydrol.2018.10.038>, 2018.

429 Leander, R. and Buishand, T. A.: Resampling of regional climate model output for the simulation of
430 extreme river flows, *Journal of Hydrology*, 332, 487 – 496,
431 <https://doi.org/10.1016/j.jhydrol.2006.08.006>, 2007.

432 Lenderink, G., Buishand, A., and van Deursen, W.: Estimates of future discharges of the river Rhine
433 using two scenario methodologies: direct versus delta approach, *Hydrology and Earth System
434 Sciences*, 11, 1145–1159, <https://doi.org/10.5194/hess-11-1145-2007>, 2007.

435 Liu, Z., Wang, R., and Yao, Z.: Climate change and its impact on water availability of large
436 international rivers over the mainland Southeast Asia, *Hydrological Processes*, 32, 3966–3977,
437 <https://doi.org/10.1002/hyp.13304>, 2018.

438 Luo, X., Wu, W., He, D., Li, Y., and Ji, X.: Hydrological simulation using TRMM and CHIRPS
439 precipitation estimates in the lower Lancang-Mekong River Basin, *Chinese Geographical Science*,

440 29, 13–25, <https://doi.org/10.1007/s11769-019-1014-6>, 2019.

441 Malik, N., Bookhagen, B., and Mucha, P. J.: Spatiotemporal patterns and trends of Indian monsoonal
442 rainfall extremes, *Geophysical Research Letters*, 43, 1710,
443 <https://doi.org/doi:10.1002/2016GL067841>, 2016.

444 Nishat, B. and Rahman, S. M. M.: Water resources modeling of the Ganges-Brahmaputra-Meghna
445 River Basins using satellite remote sensing data, *Journal of the American Water Resources
446 Association*, 45, 1313–1327, <https://doi.org/10.1111/j.1752-1688.2009.00374.x>, 2009.

447 Pervez, M. S. and Henebry, G. M.: Spatial and seasonal responses of precipitation in the Ganges
448 and Brahmaputra river basins to ENSO and Indian Ocean dipole modes: implications for flooding
449 and drought, *Nat. Hazards Earth Syst. Sci.*, 15, 147–162, <https://doi.org/10.5194/nhess-15-147-2015>,
450 2015.

451 Prakash, S., Mitra, A. K., Momin, I. M., Rajagopal, E. N., Basu, S., Collins, M., Turner, A. G., Rao,
452 K. A., and Ashok, K.: Seasonal intercomparison of observational rainfall datasets over India during
453 the southwest monsoon season, *International Journal of Climatology*, 35, 2326–2338,
454 <https://doi.org/10.1002/joc.4129>, 2015.

455 Prakash, S., Seshadri, A., Srinivasan, J., and Pai, D. S.: A new parameter to assess impact of rain
456 gauge density on uncertainty in the estimate of monthly rainfall over India, *Journal of
457 Hydrometeorology*, 20, 821–832, <https://doi.org/10.1175/JHM-D-18-0161.1>, 2019.

458 Rana, S., McGregor, J., and Renwick, J.: Precipitation seasonality over the Indian subcontinent: an
459 evaluation of gauge, reanalyses, and satellite retrievals, *Journal of Hydrometeorology*, 16, 631–651,
460 <https://doi.org/10.1175/jhm-d-14-0106.1>, 2015.

461 Ray, P. A., Yang, Y. E., Wi, S., Khalil, A., Chatikavanij, V., and Brown, C.: Room for improvement:

462 Hydroclimatic challenges to poverty-reducing development of the Brahmaputra River basin,
463 *Environmental Science & Policy*, 54, 64–80, <https://doi.org/10.1016/j.envsci.2015.06.015>, 2015.

464 Schmidli, J., Frei, C., and Vidale, P. L.: Downscaling from GCM precipitation: a benchmark for
465 dynamical and statistical downscaling methods, *International Journal of Climatology*, 26, 679–689,
466 <https://doi.org/10.1002/joc.1287>, 2006.

467 Sillmann, J., Kharin, V. V., Zhang, X., Zwiers, F. W., and Bronaugh, D.: Climate extremes indices
468 in the CMIP5 multimodel ensemble: Part 1. Model evaluation in the present climate, *Journal of*
469 *Geophysical Research: Atmospheres*, 118, 1716–1733, <https://doi.org/doi:10.1002/jgrd.50203>,
470 2013.

471 Singh, S., Kumar, R., Bhardwaj, A., Sam, L., Shekhar, M., Singh, A., Kumar, R., and Gupta, A.:
472 Changing climate and glacio-hydrology in Indian Himalayan Region: a review. Wiley
473 *Interdisciplinary Reviews: Climate Change*, 7, 393–410. <https://doi.org/10.1002/wcc.393>, 2016.

474 Singh, V. P., Sharma, N., and Ojha, C. S. P. (Eds.): *The Brahmaputra Basin water resources*, Kluwer
475 Academic Publishers, Dordrecht, Netherlands, pp. 17–34, 2004.

476 Teutschbein, C. and Seibert, J.: Bias correction of regional climate model simulations for
477 hydrological climate-change impact studies: Review and evaluation of different methods, *Journal*
478 *of Hydrology*, 456–457, 12–29, <https://doi.org/10.1016/j.jhydrol.2012.05.052>, 2012.

479 Wang, C., Ren, X., and Li, Y.: Analysis of extreme precipitation characteristics in low mountain
480 areas based on three-dimensional copulas—taking Kuandian County as an example, *Theoretical and*
481 *Applied Climatology*, 128, 169–179, <https://doi.org/10.1007/s00704-015-1692-7>, 2017.

482 Xu, R., Hu, H., Tian, F., Li, C., and Khan, M. Y. A.: Projected climate change impacts on future
483 streamflow of the Yarlung Tsangpo-Brahmaputra River, *Global and Planetary Change*, 175, 144–

484 159, <https://doi.org/10.1016/j.gloplacha.2019.01.012>, 2019.

485 Yatagai, A., Kamiguchi, K., Arakawa, O., Hamada, A., Yasutomi, N., and Kitoh, A.: APHRODITE:
486 Constructing a long-term daily gridded precipitation dataset for Asia based on a dense network of
487 rain gauges, *Bulletin of the American Meteorological Society*, 93, 1401–1415,
488 <https://doi.org/10.1175/bams-d-11-00122.1>, 2012.

489 Yucel, I. and Onen, A.: Evaluating a mesoscale atmosphere model and a satellite-based algorithm in
490 estimating extreme rainfall events in northwestern Turkey, *Nat. Hazards Earth Syst. Sci.*, 14, 611–
491 624, <https://doi.org/10.5194/nhess-14-611-2014>, 2014.

492 Zhang Y., Zheng H., Herron N., Liu X., Wang Z., Chiew, F. H. S., and Parajka, J.: A framework
493 estimating cumulative impact of damming on downstream water availability, *Journal of Hydrology*,
494 575, 612–627, <https://doi.org/10.1016/j.jhydrol.2019.05.061>, 2019.

495 **Table 1.** Detailed description of extreme precipitation indices.

496

497 **Table 1.** Detailed description of extreme precipitation indices.

Index	Descriptive name	Definition	Unit
CWD	Consecutive wet days	Maximum number of consecutive days with precipitation ≥ 1 mm	days
R10mm	Number of heavy precipitation days	Count of days when precipitation ≥ 10 mm during June, July, August, and September (JJAS)	days
R20mm	Number of very heavy precipitation days	Count of days when precipitation ≥ 20 mm during JJAS	days
Rx1d	Maximum 1-day precipitation amount	Maximum 1-day precipitation	mm
Rx5d	Maximum 5-day precipitation amount	Maximum consecutive 5-day precipitation	mm
SDII	Simple daily intensity index	Total precipitation during JJAS divided by the number of wet days (when precipitation ≥ 1 mm)	mm/day

498

499 **Figure 1.** Locations of rainfall stations in the Yarlung Tsangpo-Brahmaputra River Basin (YBRB).

500 **Figure 2.** Location of Asian Precipitation Highly Resolved Observational Data Integration Towards
501 Evaluation of Water Resources (APHRODITE) grids over the Tibetan plateau (TP), Himalayan belt
502 (HB), and floodplains (FP).

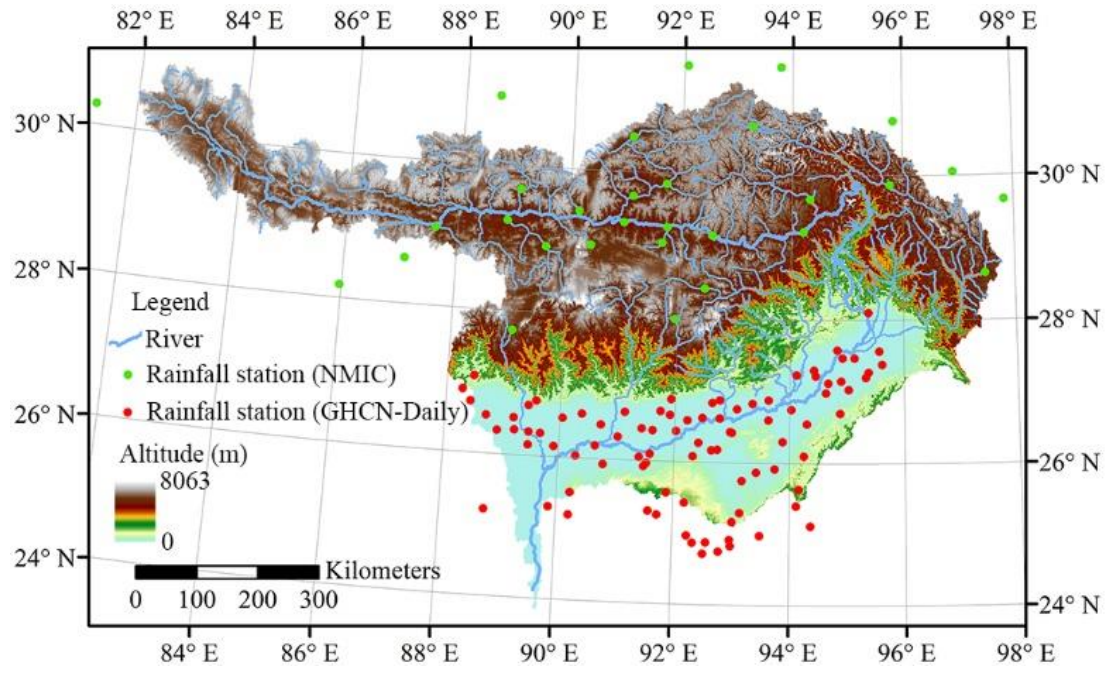
503 **Figure 3.** Box-whisker plot for (a) consecutive wet days (CWD), (b) number of heavy precipitation
504 days (R10mm), (c) number of very heavy precipitation days (R20mm), (d) maximum 1-day
505 precipitation amount (Rx1d), (e) maximum 5-day precipitation amount (Rx5d), and (f) simple daily
506 intensity index (SDII) during June, July, August, and September (JJAS) in the three different
507 physiographic zones (the TP, HB, and FP) of the YBRB derived from original and corrected
508 APHRODITE estimates.

509 **Figure 4.** Relative change rate of (a) CWD, (b) R10mm, (c) R20mm, (d) Rx1d, (e) Rx5d, and (f)
510 SDII during JJAS for original and corrected APHRODITE estimates.

511 **Figure 5.** Mean error (*ME*) of extreme precipitation indices during JJAS for validation in the three
512 different physiographic zones (TP, HB, and FP) of the YBRB.

513 **Figure 6.** Spatial distribution of mean Rx5d during JJAS in the YBRB based on (a) original
514 APHRODITE estimates, as well as (b) linear scaling (LS)-APHRODITE estimates, (c) local
515 intensity scaling (LOCI)-APHRODITE estimates, (d) power transformation (PT)-APHRODITE
516 estimates, and (e) quantile–quantile mapping (QM)-APHRODITE estimates.

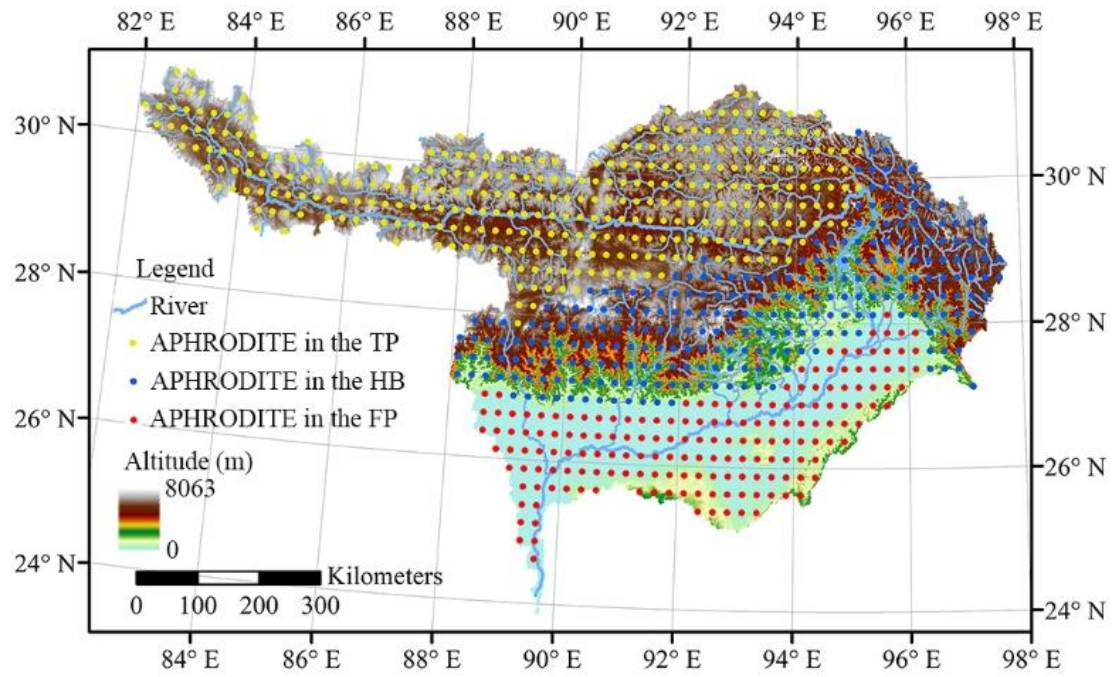
517



518

519 **Figure 1.** Locations of rainfall stations in the Yarlung Tsangpo-Brahmaputra River Basin (YBRB).

520



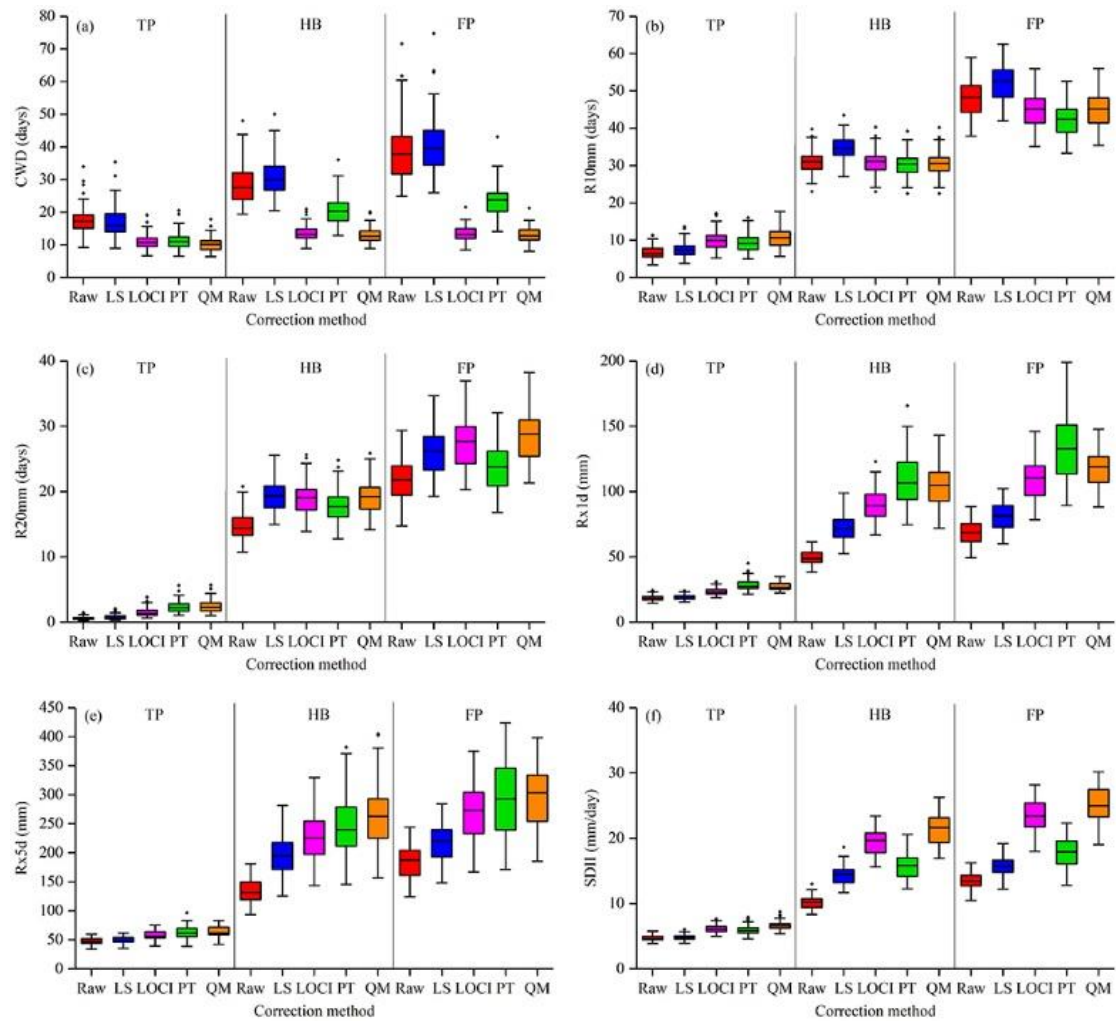
521

522 **Figure 2.** Location of Asian Precipitation Highly Resolved Observational Data Integration Towards

523 Evaluation of Water Resources (APHRODITE) grids over the Tibetan plateau (TP), Himalayan belt

524 (HB), and floodplains (FP).

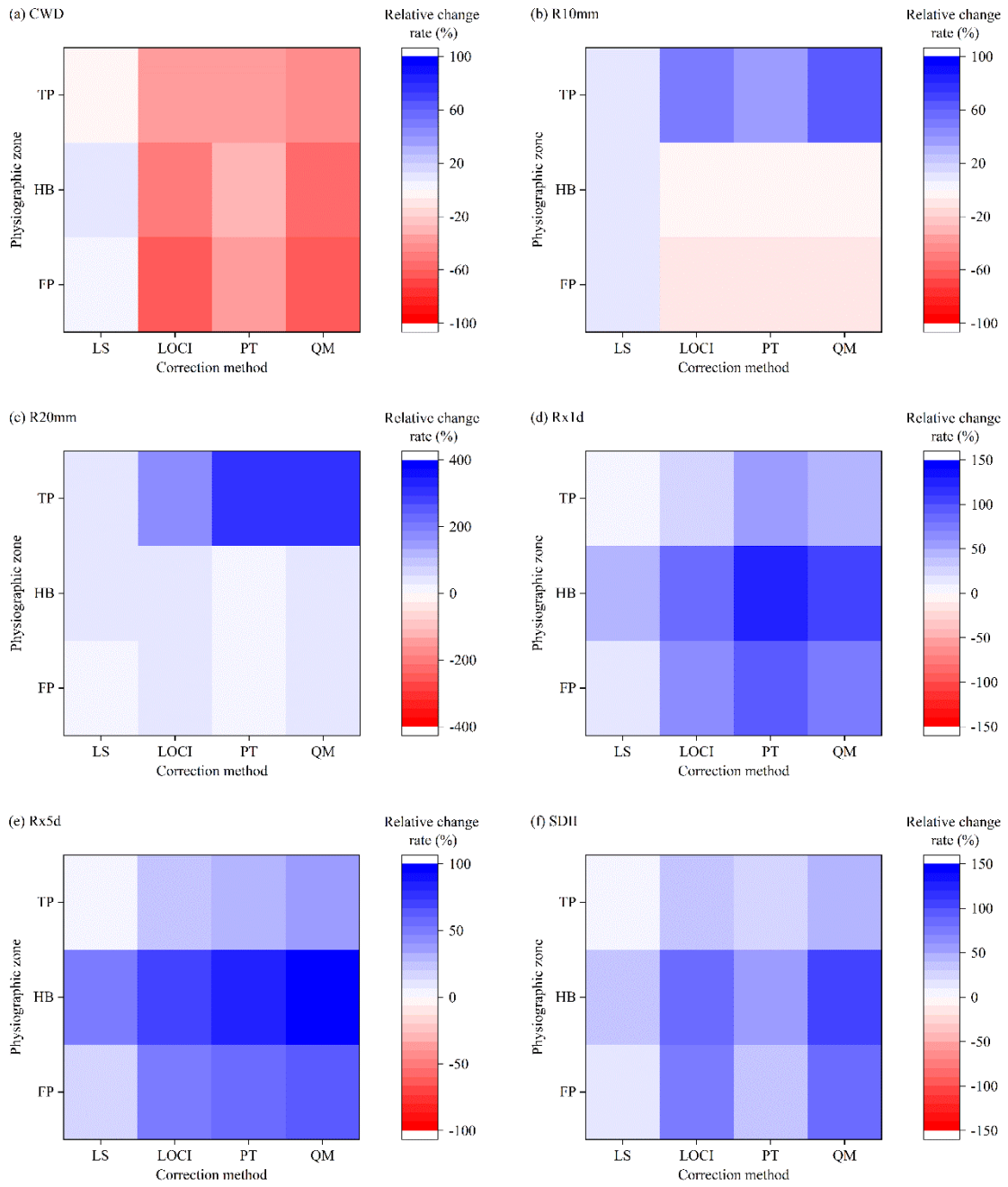
525



526

527 **Figure 3.** Box-whisker plot for (a) consecutive wet days (CWD), (b) number of heavy precipitation
 528 days (R10mm), (c) number of very heavy precipitation days (R20mm), (d) maximum 1-day
 529 precipitation amount (Rx1d), (e) maximum 5-day precipitation amount (Rx5d), and (f) simple daily
 530 intensity index (SDII) during June, July, August, and September (JJAS) in the three different
 531 physiographic zones (the TP, HB, and FP) of the YBRB derived from original and corrected
 532 APHRODITE estimates.

533

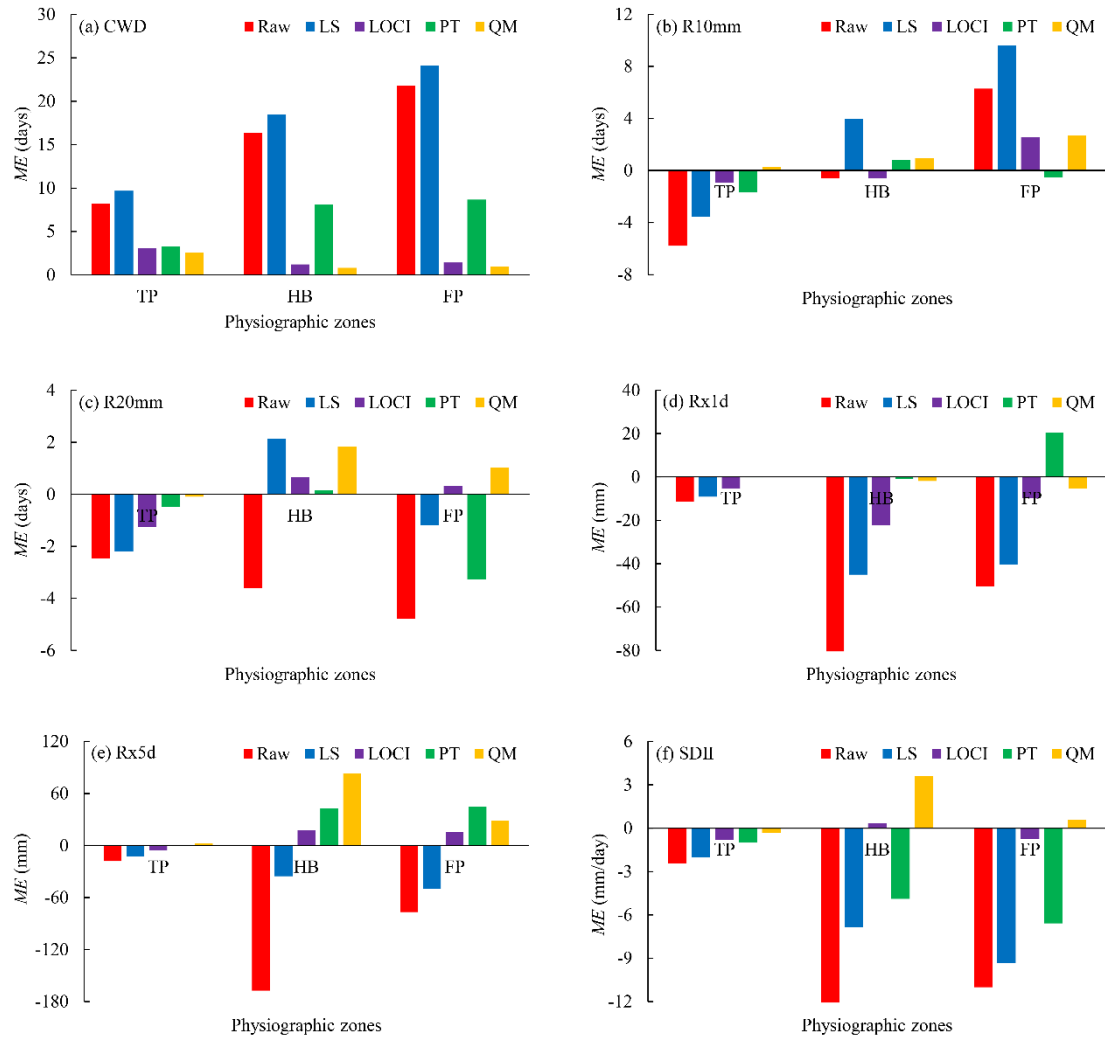


534

535 **Figure 4.** Relative change rate of (a) CWD, (b) R10mm, (c) R20mm, (d) Rx1d, (e) Rx5d, and (f)

536 SDII during JJAS for original and corrected APHRODITE estimates.

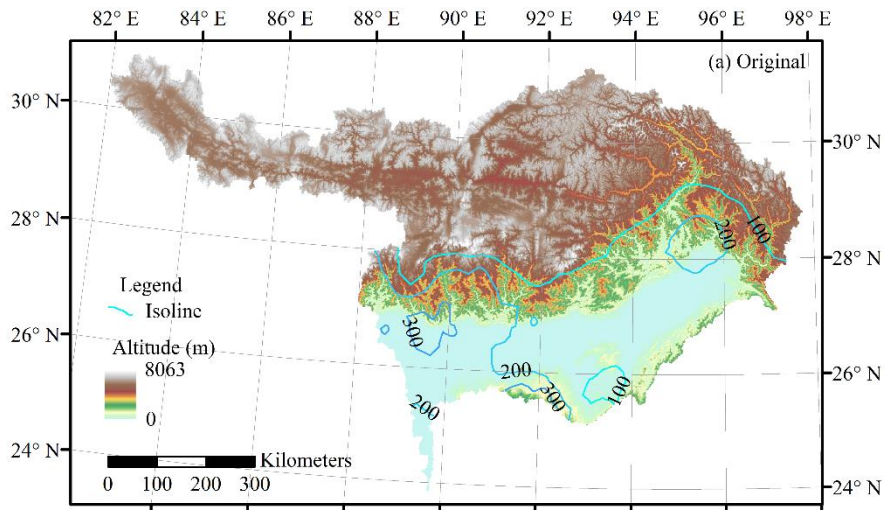
537



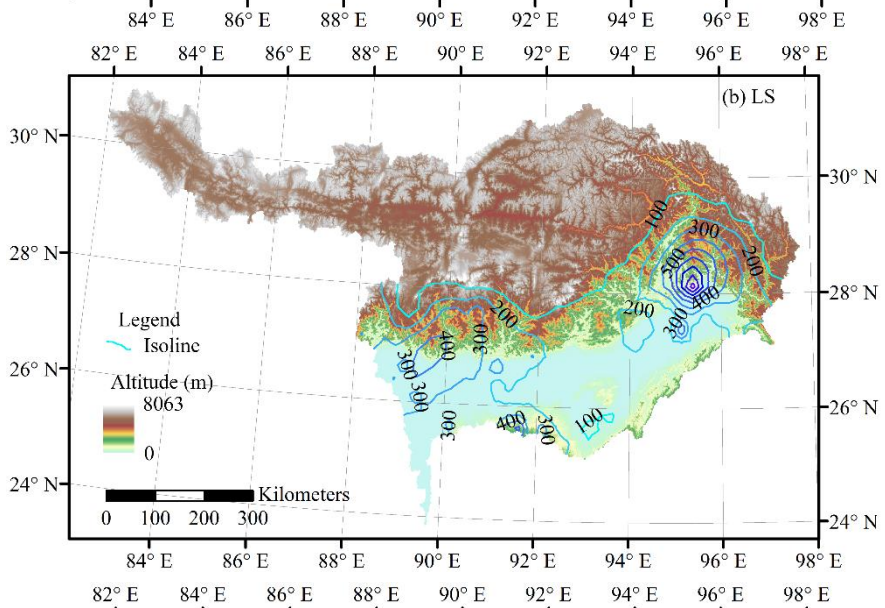
538

539 **Figure 5.** Mean error (*ME*) of extreme precipitation indices during JJAS for validation in the three
 540 different physiographic zones (TP, HB, and FP) of the YBRB.

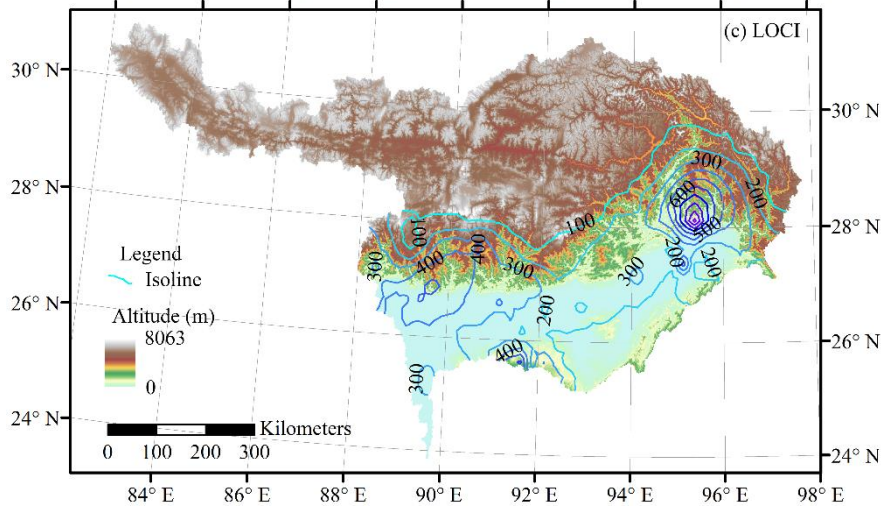
541



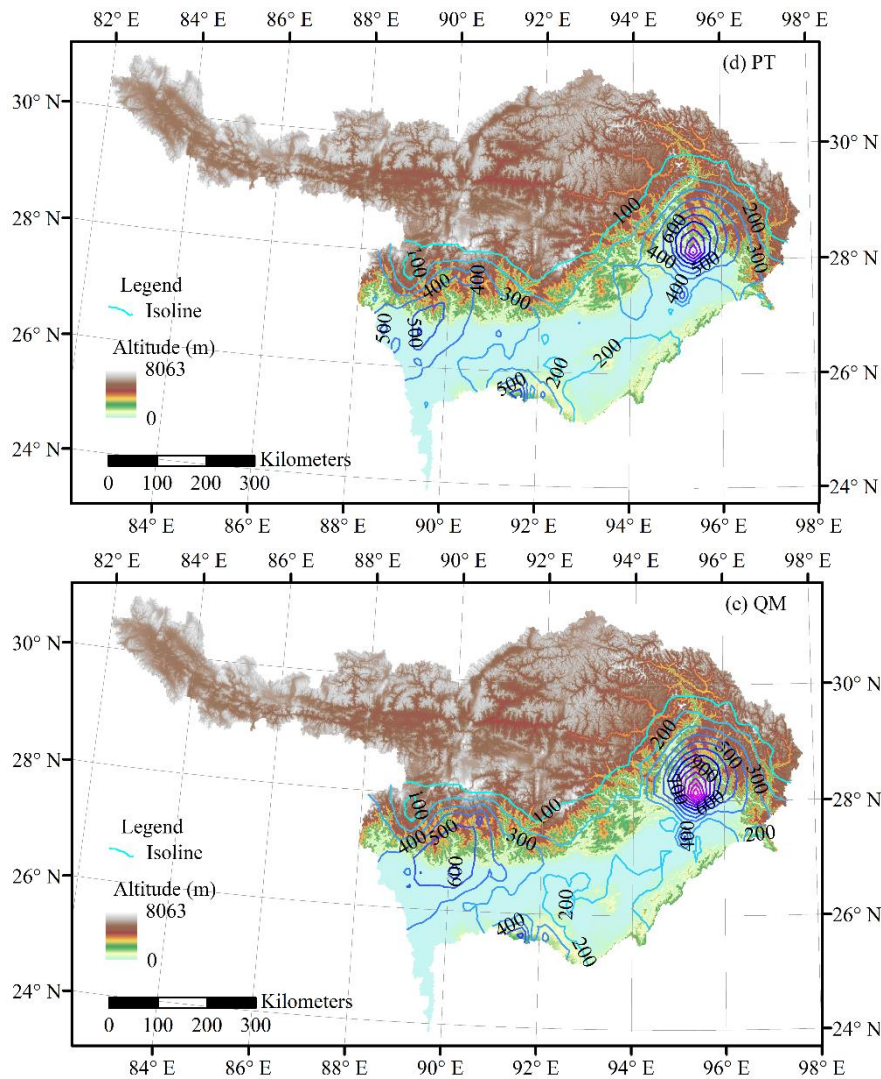
542



543



544



545

546

547 **Figure 6.** Spatial distribution of mean Rx5d during JJAS in the YBRB based on (a) original
 548 APHRODITE estimates, as well as (b) linear scaling (LS)-APHRODITE estimates, (c) local
 549 intensity scaling (LOCI)-APHRODITE estimates, (d) power transformation (PT)-APHRODITE
 550 estimates, and (e) quantile-quantile mapping (QM)-APHRODITE estimates.

551